Microcrystalline, nanocrystalline, and ultrananocrystalline diamond chemical vapor deposition: Experiment and modeling of the factors controlling growth rate, nucleation, and crystal size

P. W. May[a)] and M. N. R. Ashfold
School of Chemistry, University of Bristol, Bristol BS8 1TS, United Kingdom

Yu. A. Mankelevich
Nuclear Physics Institute, Moscow State University, 119992 Moscow, Russia

$Ar/CH_4/H_2$ gas mixtures have been used to deposit microcrystalline diamond, nanocrystalline diamond, and ultrananocrystalline diamond films using hot filament chemical vapor deposition. A three-dimensional computer model was used to calculate the gas phase composition for the experimental conditions at all positions within the reactor. Using the experimental and calculated data, we show that the observed film morphology, growth rate, and across-sample uniformity can be rationalized using a model based on competition between H atoms, CH_3 radicals, and other C_1 radical species reacting with dangling bonds on the surface. Proposed formulas for growth rate and average crystal size are tested on both our own and published experimental data for $Ar/CH_4/H_2$ and conventional 1% CH_4/H_2 mixtures, respectively. © *2007 American Institute of Physics.*
[DOI: 10.1063/1.2696363]

I. INTRODUCTION

Diamond films can be deposited using a chemical vapor deposition (CVD) process involving the gas phase decomposition of a gas mixture containing a small quantity of a hydrocarbon in excess hydrogen.[1] A typical gas mixture uses 1% CH_4 in H_2, and this produces polycrystalline films with grain sizes in the micron or tens of micron range, depending upon growth conditions, substrate properties, and growth time. It is generally believed[2,3] that the main growth species in standard diamond CVD is the CH_3 radical, which adds to the diamond surface following hydrogen abstraction by H atoms. Thus, a high concentration of atomic H at the surface in addition to CH_3 radicals is a prerequisite for successful microcrystalline diamond (MCD) deposition. By increasing the ratio of methane in the standard CH_4/H_2 gas mixture from 1% to ~5%, the grain size of the films decreases, and eventually becomes of the order of hundreds down to tens of nm. Such nanocrystalline diamond (NCD) films (often termed "cauliflower" or "ballas" diamond) are smoother than the microcrystalline ones, but have larger numbers of grain boundaries that contain substantial graphitic impurities. With further addition of CH_4, the films become graphitic.

Recently, so-called ultrananocrystalline diamond (UNCD) films have become a topic of great interest, since they offer the possibility of making smooth, hard coatings at relatively low deposition temperatures, which can be patterned to nanometer resolution.[4,5] These differ from NCD films,[6] since they have much smaller grain sizes (~2 −5 nm), and have little or no graphitic impurities at the grain boundaries. Most reports of the deposition of these films describe using a microwave (MW) plasma CVD reactor and gas mixture of 1% CH_4 in Ar, usually with addition of 1% −5% H_2.[4]

We have previously reported the use of similar $Ar/CH_4/H_2$ gas mixtures to deposit NCD (or UNCD) in a hot filament (HF) reactor,[7] with the compositional diagram for mixtures of Ar, CH_4, and H_2 being mapped out corresponding to the type of film grown. For the majority of the composition diagram, diamond films are deposited only in a very narrow region around $[CH_4]/([CH_4]+[H_2]) \sim 0.5\%$ −6%, with UNCD films being deposited only in the region of the MCD/"no-growth" boundary.

Originally it was suggested[8] that the C_2 radical played an important role in the growth mechanism for UNCD. However, recent work by ourselves[9,10] and others[11] has shown that C_2 is only a minority species close to the substrate surface and plays no significant role in growth. In our previous article,[10] we used a two-dimensional model of the gas chemistry, including heat and mass transfer, in our HF reactors to understand the experimental observations. The conclusions led to a generalized mechanism for the growth of diamond by CVD which was consistent with all experimental observations, both from our group and from others in the literature.

The proposed mechanism involves competitive growth by all the C_1 radical species that are present in the gas mixture close to the growing diamond surface. Previous models only considered CH_3 since this is the dominant reactive hydrocarbon radical in standard H_2-rich CVD gas mixtures. However, we found that in HFCVD reactors at high filament temperatures (e.g., $T_{fil} \sim 2700$ K), the concentration of the other C_1 radical species, in particular C atoms, near the growing diamond surface can become a significant fraction (~5%) of that of CH_3, and so may contribute to the growth

---

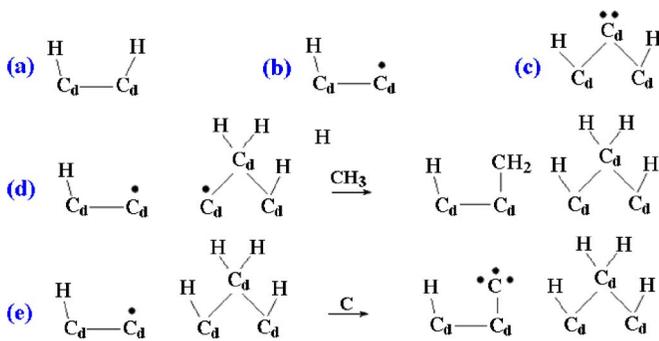a)Electronic mail: paul.may@bris.ac.uk

101, 053115-1

FIG. 1. Schematic diagram of the various (100)-(2×1) dimer surface and bridge sites important for diamond growth and renucleation. (a) A hydrogen terminated diamond surface. (b) A surface radical site C_d^*. (c) A surface biradical site C_d^{**}. (d) A different type of surface biradical site, C_d^*-C_d^*, followed by its reaction with methyl to give a CH_2 surface group (Ref. 16). (e) The radical site also reacts with a C atom (or CH radical, not shown) to give a reactive surface adduct C_d^{**}.

process. C atoms as gas-phase precursors of diamond films have been considered before for HFCVD,[12] microwave CVD,[13] and plasma arc jet reactors,[12,14,15] however, they were neglected in favor of CH_3.

In the model, abstraction of surface H atoms by gas phase atomic H are the reactions which drive the chemistry of growth. The various types of surface radical that result from abstraction are shown in Fig. 1. We proposed that CH_3 remains the major growth species, and if this adds to a surface biradical site, C_d^*-C_d^*, defined as two surface radical sites adjacent to one another, see Fig. 1(d), the "dangling bonds" on the surface are terminated and stabilized.[15] For typical diamond CVD conditions, the fraction of available biradical sites is ~10 times lower than that of radical sites [Fig. 1(b)], but CH_3 cannot add to the more abundant radical sites due to steric hindrance.[16] Further hydrogen abstraction converts the surface CH_3 groups into bridging CH_2 groups, and repetition of this process allows the CH_2 groups to migrate across the surface until they meet a step edge, at which point they will extend the diamond lattice leading to large regular crystals, and a MCD film, as usual.[10] Thus, the prerequisites for MCD film formation are high H concentration (to generate sufficient surface biradical sites), high CH_3 concentration, and the rapid migration across the surface of CH_2 groups (catalyzed by H atom abstractions).

However, as well as CH_3 addition, we assumed that C atoms or CH radicals (and also CH_2 but these have been neglected since their number density close to the substrate surface is much lower) could also be adsorbed on the surface. Due to their smaller size, atomic C and CH have less steric hindrance and can add to both surface biradical sites and radical sites (see Fig. 1). Thus, even for low C atom concentrations $[C]/[CH_3] \sim 0.1$, their contribution to the growth rate can become important since they can add to the more abundant radical sites. The resulting adduct structure C_d^{**} [see Fig. 1(e)] would remain reactive since it would still contain dangling bonds, making this a very high energy site. The most likely fate for such reactive surface sites, considering that they are surrounded by a gas mixture containing a high concentration of H atoms and H_2 molecules, is that they are rapidly hydrogenated to CH_2. If so, the subsequent reac-

tions will be indistinguishable from attachment and growth by methyl. However, other possible fates for the reactive surface adducts are reaction with other gas-phase hydrocarbon radicals CH_x or restructuring of the surface. The role of such adducts as an initiator of renucleation processes requires additional theoretical study. It should be noted that a C surface atom with two dangling bonds [C_d^{**}, Fig. 1(c)] could also be created by an alternative process as a result of two successive hydrogen abstraction reactions on the same CH_2 surface group. The probability of such a process could be low, but not negligible, as it would be similar to that of analogous gas phase reaction rates (e.g., $H+CH_2 \rightarrow CH+H_2$ has a rate constant of 2.70×10^{-10} cm^3 s^{-1} at 1123 K).[17]

For the typical conditions used to deposit MCD/NCD and UNCD in a variety of different diamond CVD reactors (including MW and HF CVD reactors), the reactions of the surface adducts with atomic hydrogen which lead to continuous normal diamond growth are much more frequent events than the reactions with CH_x which ultimately could lead to renucleation. As long as the surface migration of CH_2 (induced by H abstractions) is much faster than adsorption of CH_3, the aggregation of CH_2 bridge sites into continuous chains (void filling) will provide normal layer-by-layer {100} diamond growth.[16] But as the ratio of gaseous CH_x/H increases, the initiation of next layer growth could proceed before all the voids in the current layer are filled. Thus, depending upon the gas mixture and reaction conditions used, the relative concentrations of each of these species close to the growing diamond surface (e.g., $[H]/[CH_3]$, $([C]+[CH])/[CH_3]$) determine the probability of a renucleation event occurring and average crystal sizes, $\langle d \rangle$, and hence, the morphology of the subsequent film, be it MCD, NCD, or UNCD.

In this article we shall present further experimental and calculated data to support and refine the proposed mechanism outlined earlier. In our previous article[10] we examined the role of different gas compositions upon UNCD growth. We now keep the gas feed mixture constant and compare the experimental measurements for the across-substrate uniformity of UNCD growth rate, crystal morphology, and film properties with those predicted by our model. We shall also present quantitative estimations of $\langle d \rangle$ and the growth rate, G, for {100} diamond growth, and thereby show that we can extend our model to offer a general unifying description of the growth and nucleation behavior for diamond that is consistent with deposition of MCD, NCD, and UNCD.

II. EXPERIMENT

Films were deposited using a standard HF reactor operating at a pressure of 100 Torr using high purity Ar, CH_4, and H_2 as source gases. Mass flow controllers were used to control the ratios of the three gases. $[Ar]/([Ar]+[H_2])$ was kept constant at 80% and that of $[CH_4]/([H_2]+[CH_4])$ at 1.5%, which puts it in the UNCD growth region of the Ar/CH_4/H_2 composition diagram.[7] The filament was made from 0.25 mm-diameter Ta metal, wound around a 3 mm-diameter core to produce a 2 cm-long coil that was positioned 5.5 mm from the substrate surface. The filament temperature was kept con-

TABLE I. The gas-surface reactions included in the model, with rate coefficients given by $k = k_0 T_{ns}^{0.5} \exp(-E/T_s)$, where T_s is the substrate temperature, T_{ns} is the gas temperature just above the substrate, and E is the activation energy in Kelvin. C_d^* means a surface radical site (a single dangling bond) and $C_d^* - C_d^*$ means a surface biradical site (see Fig. 1).

Number	Reaction	k_0 (cm^3 s^{-1})	E (K)	Reference
$R1$	$H + C_d H \rightarrow H_2 + C_d^*$	3.2×10^{-12}	3430	30
$R(-1)$	$H_2 + C_d^* \rightarrow H + C_d H$	3.2×10^{-13}	7850	Detailed balancing
$R2$	$H + C_d^* \rightarrow C_d H$	9.6×10^{-13}	0	30
$R3$	$CH_3 + C_d^* - C_d^* \rightarrow CH_2 C_d - C_d H$	2.4×10^{-13}	0	30
$R4$	$C_2 H_2 + C_d^* - C_d^* \rightarrow C_d C_2 H_2 C_d$	$< 1.2 \times 10^{-14}$	0	Estimation (Ref. 31)
$R5$	$CH_2 + C_d^* \rightarrow CH_2 C_d$	2.4×10^{-13}	0	As $R3$
$R6$	$CH + C_d^* \rightarrow CHC_d$	2.4×10^{-13}	0	As $R3$
$R7$	$C + C_d^* \rightarrow CC_d$	2.4×10^{-13}	0	As $R3$

stant at 2400 °C and monitored using a two-color optical pyrometer. The substrate was single crystal Si (100) which had been manually abraded prior to deposition using 1−3 μm diamond grit, and then ultrasonically cleaned with propan-2-ol. The substrate sat on a separate heater to give additional uniform heating and to maintain it at a temperature of ~850−900 °C (also measured using the optical pyrometer). Typical deposition times were 8 h. After deposition the films were analyzed by laser Raman spectroscopy, and both scanning and transmission electron microscopy (SEM and TEM).

III. MODELING

In our previous article,[10] we have carried out serial calculations for different methane fractions in H_2/Ar mixtures using a two-dimensional model with coordinates of r (radial distance from the center of the substrate to the edge) and z (vertical distance from the substrate to the filament. We now keep the gas feed mixture constant and use a three-dimensional (3D) model, which is much more computationally time consuming, but more accurately describes the geometry of the hot region of coiled wire and the spatial profiles of species concentrations and growth rates. The 3D model has been specifically tailored to a reactor of this geometry.[15] The input parameters for the model were taken from the experimental values: pressure 100 Torr, filament temperature 2400 °C, and $Ar/H_2/CH_4$ gas flows, as appropriate. The model comprises three blocks, which describe (i) activation of the reactive mixture (i.e., gas heating and catalytic H atom production at the filament surface), (ii) gas-phase processes (heat and mass transfer and chemical kinetics), and (iii) gas-surface processes at the substrate.

The 3D shape of the experimental filament (a coiled wire) was approximated in rectangular (x, y, z) coordinates as six parallel filaments (in the y direction) bounding the equivalent cylindrical hot volume $-1.5 < x < 1.5$ mm, $-10 < y < 10$ mm, $5.5 < z < 8.5$ mm, where the z axis is perpendicular to the substrate surface and the filament axis, and axis x is parallel to the substrate surface and perpendicular to the filament axis. The point $(0, 0, 0)$ corresponds to the substrate center.

The gas-phase chemistry and thermochemical input is taken from the GRI-Mech 3.0 detailed reaction mechanism for C/H/Ar gas mixtures.[17] As in previous studies[7,18–20] the

conservation equations for mass, momentum, energy, and species concentrations, together with appropriate initial and boundary conditions, thermal and caloric equations of state, are each integrated numerically until steady-state gas temperature and radicals distributions are attained. (It should be noted that due to the limits of computation time, it is not possible to reach steady state conditions for some of the slower reacting species, as discussed later.) This process yields spatial distributions of the gas temperature, T_{gas}, the flow field, and the various species number densities and mole fractions. The incorporation of gas-surface reactions (see Table I), involving H abstraction to form surface sites, and the subsequent reactions of these sites with H and hydrocarbon radicals, serve to alter the gas composition close to the surface. The main effect of these reactions is to reduce the H atom concentrations directly above the growing diamond surface, which in turn affects the hydrocarbon radical concentration and has major implications for subsequent growth.

Additional tests of our model were carried out using the experimental data from another group,[29] who used a commercial multifilament CVD reactor to measure growth rates and average crystal sizes as a function of the gas pressure, for MCD growth conditions using conventional CH_4/H_2 gas mixtures. To model this system, we used a two-dimensional model, with rectangular (x, z) geometry. The z coordinate is
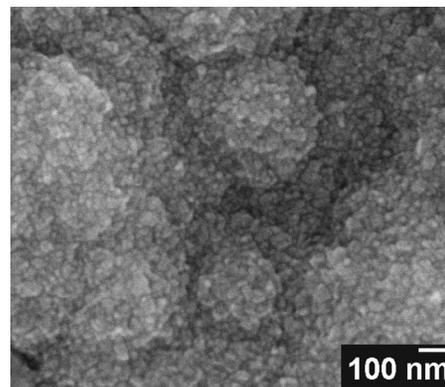

FIG. 2. A high magnification SEM photo of the UNCD surface grown for 7 h in a HFCVD reactor using a process pressure of 100 Torr, filament temperature 2400 °C and a gas mixture with $[Ar]/([Ar]+[H_2]) = 80\%$ and $[CH_4]/([H_2]+[CH_4]) = 1.5$. The film shows no faceting, but instead a dense, granular structure composed of agglomerations of smaller nanograins. TEM imaging shows the size of the nanograins to be < 10 nm.
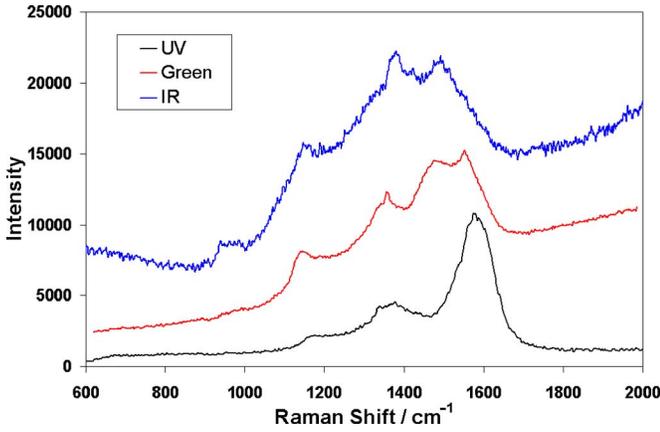
FIG. 3. Laser Raman spectra from an UNCD film grown using the conditions described in Fig. 2. The spectra have been offset vertically for clarity. Different features become apparent at different laser excitation wavelengths. For ultraviolet (325 nm) excitation (lower spectrum), the 1150 cm^{-1} peak is only a small shoulder in the spectrum, and there is a very small 1332 cm^{-1} diamond peak. For green (514 nm) excitation (middle), the 1150 cm^{-1} peak has increased in intensity, but the diamond peak has now disappeared underneath the D band. For infrared (785 nm) excitation, (top) the D and G peaks now dominate the spectrum and the 1150 cm^{-1} peak is still very evident. The feature around 950–1000 cm^{-1} in the infrared-excited spectrum is the second-order peak from the Si substrate.

perpendicular to the plane of the substrate and filaments, while the x coordinate is parallel to the substrate surface and perpendicular to the filament axis. The length of the filaments (along the y-axis) is assumed to be much larger than other characteristic sizes and gaps in the reactor.

IV. RESULTS

The variation of film morphology and properties with varying gas composition have been presented previously,[10] so in this article we shall restrict our discussion to the spatial uniformity for one set of growth conditions. The films grown in our HF reactor under the growth conditions mentioned in Sec. II, earlier, satisfied a number of criteria consistent with being UNCD. First, the films showed no evidence of facets, even at very high magnification (see Fig. 2). Second, we observed the presence of the 1150–1190 cm^{-1} Raman line (see Fig. 3), which has been attributed[21] to sp^2 carbon in

FIG. 5. A Raman spectrum (325 nm) taken at the center $(0, 0, 0)$ of a diamond/UNCD film grown with the same conditions as Fig. 2, but with $[CH_4]/([H_2]+[CH_4])=3\%$, showing the five peaks used to fit the spectrum. For this particular fit the "1450" peak needed to be shifted to ~1490 cm^{-1}.

trans-polyacetylene-like molecules trapped at the nanograin boundaries. This peak is often considered as being a signature for UNCD, despite its origin being sp^2 carbon. Third, TEM analysis revealed the films to be composed of randomly oriented crystals with grains <10 nm in size, with lattice spacings consistent with that of diamond. The growth rate of the UNCD films was low, around 0.1 μm h^{-1} in the center of the substrate directly beneath the HF $(0, 0, 0)$ and nonuniform, with a marked drop-off in growth rate with distance from the substrate center (see Fig. 4).

More detailed Raman analysis is shown in Figs. 5 and 6, for a film grown using $CH_4/(CH_4+H_2)=3\%$, which is at the boundary of the diamond/UNCD region. The spectrum shown in Fig. 5 reflects this, as the diamond peak at 1332 cm^{-1} is more prominent than in the spectrum in Fig. 3. Figure 5 illustrates how the spectrum has been fitted using five peaks, including the D (centered ~1375 cm^{-1}), G (~1583 cm^{-1}), diamond (1332 cm^{-1}), and "UNCD" peaks (~1170 cm^{-1}). The fifth peak, often centered ~1450 cm^{-1} (but which can be shifted to almost 1500 cm^{-1}), is necessary to obtain a reasonable fit to the overall data, and has been assigned[21] as a companion mode to the 1170 cm^{-1} peak. The peak positions, heights, widths, and the background are all
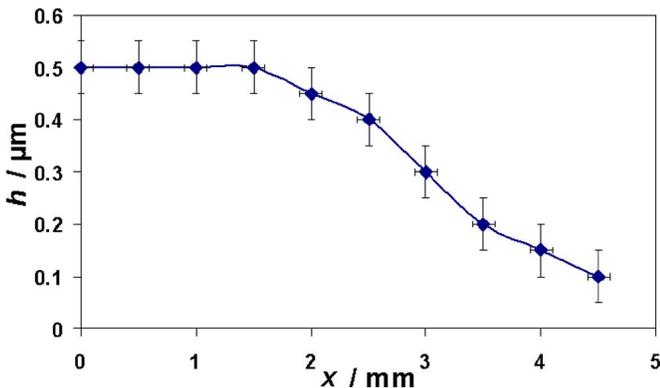

FIG. 4. Thickness, h, of the UNCD film (deposition conditions given in Fig. 2) measured by cross-sectional SEM, as a function of distance from the center of the substrate in the x direction (perpendicular to the axis of the filament).
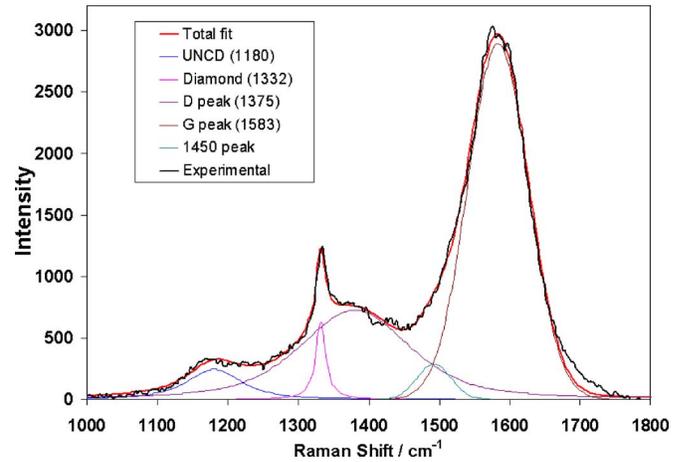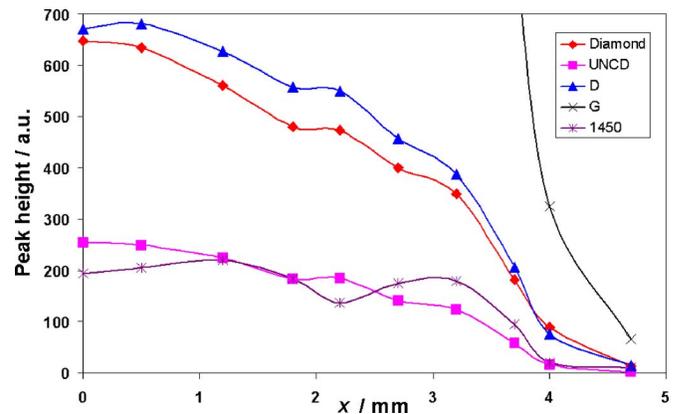

FIG. 6. The heights of the fitted Raman peaks from Fig. 5 as a function of distance from the center of the substrate, x.

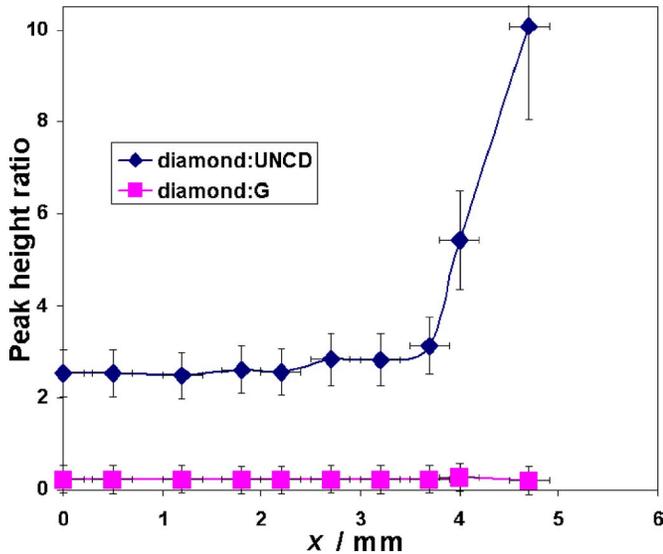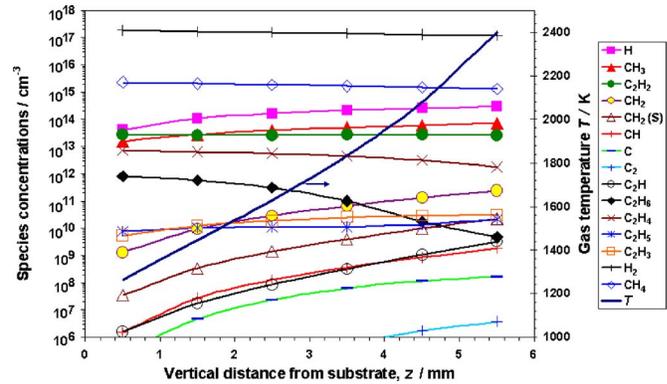FIG. 7. Raman peak height ratios from Fig. 6 as a function of x.

FIG. 8. Concentrations of various gas phase species as a function of z, the vertical distance between the substrate center ($z=0$) and the filament ($z=5.5$ mm), as well as the variation of the gas temperature, T. The calculation was performed using values of Q and ΔT so as to fit the experimental growth rates shown in Fig. 4, for a process pressure of 100 Torr, filament temperature 2400 °C and a gas mixture with $[Ar]/([Ar]+[H_2])=80\%$ and $[CH_4]/([H_2]+[CH_4])=1.5\%$.

variables in the fitting procedure. Figure 6 shows the heights of the various peaks plotted as a function of x and the falling intensities reflect the decreasing thickness of the film. Figure 7 shows the ratio of the diamond-peak height to that of both the UNCD peak and the G peak, again as a function of x. Although the diamond peak: G peak ratio stays roughly constant, it can be seen that at a distance of ~3.5 mm from the substrate center the diamond peak:UNCD-peak ratio begins to rise rapidly. This shows that the ratio of nanograined material to MCD in the films is decreasing further from the filament, until beyond a distance of ~4 mm (where from Fig. 6 the UNCD peak height has fallen to almost zero) the film can no longer be considered UNCD but predominantly MCD. A plot of peak area ratios (not shown) provides identical trends to those in Fig. 7, with the area ratio of diamond peak:UNCD peak staying constant until $x=~4$ mm, and then rapidly increasing.

Modeling of the gas phase chemistry allows gas temperature and gas phase concentrations to be calculated as a function of (x, y, z) coordinates. The distance between the bottom of the hot filament and the substrate was $z~5.5$ mm, consistent with that in the experiments. In the model for the HFCVD reactor there are two reactor specific parameters, which are not well determined. These are (i) the temperature discontinuity ΔT (the difference between filament temperature T_f and the gas temperature near the filament, T_{nf}) and (ii) the catalytic H_2 dissociation rate Q on the filament surface (i.e., the net production of H atoms per second per unit area). In our previous article,[10] we used values of ΔT and Q similar to those adopted in previous HFCVD reactor studies in standard 1% CH_4/H_2 mixtures at gas pressures of 20 Torr.[19,20] As pointed out in Ref. 10, the Q values in the mixture now under study (20% H_2/80% Ar plus ~0.3% CH_4 at 100 Torr of total pressure) could be significantly lower as a result of the gradual buildup of graphitic layers on the filament surface during growth, reducing its catalytic efficiency. In this study, we found we must reduce Q by about two orders of magnitude to a value of $Q=6\times10^{17}$ cm^{-2} s^{-1} in order to provide the observed experimental growth rates (~0.1 μm h^{-1} at

the substrate center). According to the Smoluchowski equation,[22] ΔT decreases with pressure, and so for a process pressure of 100 Torr we have used $\Delta T=300$ K instead of the previous value of ~500 K for $T_f~2700$ K at 20 Torr. As a result, the calculated concentrations of H and CH_x ($x<3$) for these new values are significantly lower than in Ref. 10. As a further consequence, we have needed to refine our previous growth model from that outlined in the introduction to account for the fact that the concentrations of C_1 species near the growing diamond surface are not as high (compared to CH_3) as previously assumed,[10] see later.

As an example, the calculated gas phase species distribution between the filament and substrate ($0<z<5.5$ mm, $x=0$) is shown in Fig. 8. Diffusion coefficients D_i for a 20% H_2/80% Ar mixture at gas pressure $p=100$ Torr, calculated using species' Lennard-Jones parameters[23] and approximated as $D_i=a_iT^{1.7}/p$,[24] (where T is the gas temperature and a_i is a constant for species i) are significantly lower than the D_i values in the widely used 1% CH_4/H_2 mixture at 20 Torr. Thus, we observe much steeper species gradients in z as well as in lateral x directions for our 20% H_2/80% Ar mixture. It should be noted that some of the species (e.g., C_2H_x) with slower production and loss rates have still not reached their steady-state equilibrium concentrations values within the computationally available propagation times of <1 s. This is a known problem when determining the concentrations in CVD reactors of these species, both theoretically and experimentally. For example, it has been shown[25] that measured C_2H_2 concentrations in HFCVD reactors are established on a timescale of tens of seconds, which is much longer than can be presently calculated. Thus, the concentration of some of these slower C_2H_x species will be underestimated in our model. Figure 8 shows that the concentration of atomic H near the surface decreases as a result of gas-surface reactions. Since reactions with atomic H generate hydrocarbon radicals, this drop in [H] has the effect of decreasing the concentrations of *all* the other gas phase radicals near the surface. However, the depletion of CH_x concentration specifically by gas-surface chemical reactions is negli-

gible on this scale. In other words, the surface is an important sink only for H atoms and does not provide a significant loss mechanism for any of the hydrocarbon species.

As in standard MCD growth conditions, we see in Fig. 8 for our hot filament UNCD growth conditions (see Sec. II) that near to the growing surface there is a relatively high concentration of CH_3 but much lower concentrations of all the other C_1 and C_2 radicals. With CH_3 being the dominant reactive hydrocarbon radical, diamond growth will occur via three basic reactions $(R1)-(R3)$ shown in Table I. Reaction $(R1)$ is the abstraction of a terminating hydrogen by a gas phase H atom, producing a reactive surface radical site. The reverse of this reaction $[R(-1)]$ together with $(R2)$ lead to the additions of a H atom to the surface radical site, thereby returning the diamond surface to its normal hydrogen-terminated state with a base CH_2 surface group. Reaction $(R3)$ is the methyl addition step which propagates the diamond structure and maintains the symmetry of the lattice.

Depending upon which C_1 species adds to the substrate, there are different rate laws (with correspondingly different rate constants) which govern the kinetics, and hence, the growth rate. It is possible to estimate the contribution to the growth rate, G (in μm h^{-1}), of the important C_1 species, using formulas stated in Ref. 26,

$$G_{CH_3} = 3.8 \times 10^{-14} T_{ns}^{0.5}[CH_3]R^2, \tag{1}$$

$$G_{CH_x} = 3.9 \times 10^{-14} T_{ns}^{0.5}[CH_x]R, \tag{2}$$

where T_{ns} is the gas temperature near the substrate (obtained from the modeling results in Ref. 10) and CH_x is for $x=0, 1, 2$. R is the fraction of surface radical sites given by $R=C_d^*/(C_d^*+C_dH)$, where C_d^* and C_dH are the respective densities of open- and hydrogen-terminated surface sites. (The probability of the surface site becoming a biradical site is, therefore, R^2.) This fraction, R, mainly depends on the rate constants for the surface H abstraction and addition reactions, and can be calculated using the data and following the procedure outlined in our previous article.[9] For example, neglecting the effects of CH_x upon radical site density R, so that

$$R=1/\{1 + k_2/k_1 + k_{-1}[H_2]/(k_1[H])\} \tag{3}$$

and using the known dependences of the coefficients k_i (from Table I) we obtain

$$R = 1/\{1 + 0.3 \exp(3430/T_s) + 0.1 \exp(-4420/T_s)[H_2]/[H]\}. \tag{4}$$

Here T_s is the substrate temperature in Kelvin, with $[H]$ and $[H_2]$, respectively, being the atomic and molecular hydrogen concentrations near the substrate.

Given the concentrations of species near the surface shown in Fig. 8, two mechanisms which affect the normal diamond structure propagation can be highlighted:

(a)   The appearance of a surface C atom with *two* dangling bonds C_d^{**}, followed by adsorption of other gas-phase hydrocarbon radicals or restructuring of the surface.
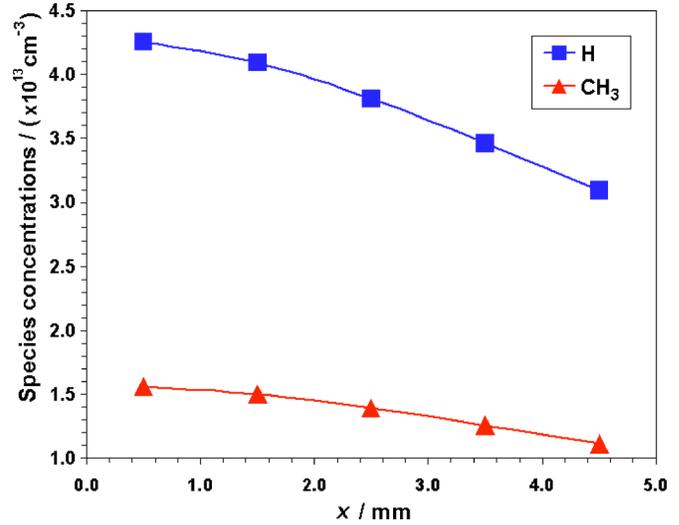

FIG. 9. Calculated $[CH_3]$ and $[H]$ concentrations just above the substrate ($z=0.5$ mm) as a function of distance x from substrate center.

The possibility of such renucleation mechanisms requires additional study.

(b)   The growth of the next layer before filling all the voids of the current layer, which can occur at high CH_3 addition rate,[16] or more exactly, at elevated gaseous $\Sigma CH_x/H$ ratios, $x<4$.

For an average crystal size $\langle d \rangle$, if we now assume that a surface CH_2 group (created after adsorption of gaseous CH_x) has sufficient time to migrate an average distance $\sim 0.5\langle d \rangle$ before the next adsorption of gaseous CH_x occurs, they will aggregate into continuous chains. This means that for monolayer growth on the (100) surface, CH_x ($x<4$) addition events to a biradical site must be less frequent than CH_2 surface group migration over a distance $0.5\langle d \rangle$. If this were not true, island growth or nonuniform growth (as opposed to normal layer-by-layer growth) would be observed, and so this limits the maximum size of crystals. H abstraction reactions are needed for CH_2 surface migration[16] and thus migration of a distance $0.5\langle d \rangle$ will require $\sim 0.5\langle d \rangle/l$ abstraction reactions, where l is a characteristic distance, e.g., for a (100) diamond surface the average distance between C atoms is $l \sim 0.25$ nm.[27] Comparing the frequency of these migration processes with the CH_x addition frequency, we can estimate the average crystal size corresponding to the deposition conditions, in particular, to the ratio of $[H]/[\Sigma CH_x]$ above the substrate and the substrate temperature, T_s,

$$k_1[H](1 - R)l/(0.5\langle d \rangle) \geq k_3[\Sigma CH_x]R^2. \tag{5}$$

Thus we have the limit of the normal growth length (i.e., the crystal size) as

$$\langle d \rangle = 2k_1[H](1 - R)l/(k_3[\Sigma CH_x]R^2). \tag{6}$$

Using Eq. (6) with Eqs. (1)–(4), average crystal sizes and growth rates can be calculated and compared with experimental data. Figures 9 and 10 show the distribution of CH_3 and H species concentrations along the x axis just above the substrate ($z=0.5$ mm), together with the calculated growth rates and crystal sizes, respectively. The growth rate can be
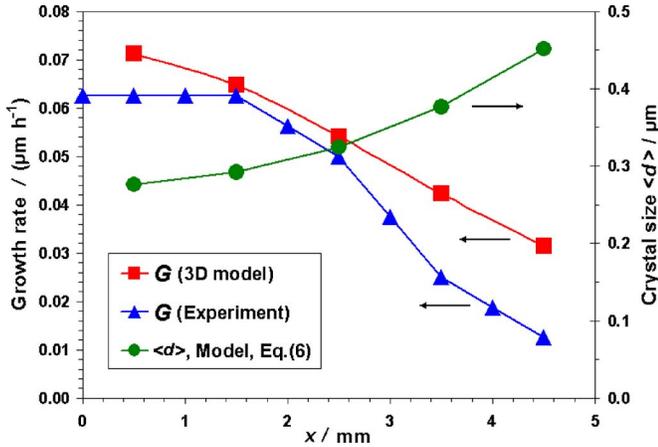
FIG. 10. Total growth rate and average crystal size calculated as a function of distance x from the center of the substrate.

FIG. 11. Experimental measurements of growth rate (▲), along with our simulation of the growth rate (●) as a function of process pressure, p, for the diamond growth conditions published in Ref. 29. Also shown is the growth rate due to CH_3 (♦) and that due to the total of the other C_1 species (■), both calculated using Eqs. (1) and (2). The experimental crystal size (×) shows a marked dependence on pressure, and the Raman spectra in Ref. 29 show that the film quality improved as the pressure was reduced from 40 to 14 Torr, but then the grain size rapidly decreased until by 2 Torr the films had become smooth and nanocrystalline, with the Raman spectra showing the 1170 cm^{-1} peak characteristic of UNCD. Also shown is the crystal size (+) calculated using Eq. (6) which closely follows the experimental data.

seen to drop off as x increases, i.e., the film gets thinner towards the edge of the substrate. Note that the film thickness at the substrate edge, calculated as $G(x=4.5 \text{ mm}) \times t$, after deposition time $t=8$ h, does not exceed the crystal size $\langle d \rangle$. This indicates that at the edge the film can still be considered as isolated crystals, whereas at the substrate center, where $G(x=0) \times t$ is higher than $\langle d \rangle$, the film is continuous. These observations are consistent with the across substrate uniformity in growth seen previously in experiment (Fig. 4). It is also consistent with the observations of other workers that MCD and UNCD can be deposited simultaneously in different places on the same substrate, because of local variations in renucleation rate.[28] Some areas of the film (towards the edges of the wafer in our system) would be more microcrystalline, while other near the center would be NCD/UNCD.

As mentioned earlier, we have used the same simulation procedure with published data for a different multifilament CVD system from the Erlangen-Nurnberg University group that has been used to grow MCD and NCD films.[29] For their growth conditions at $T_f = 2673$ K and $T_s = 1123$ K, using a 1% CH_4/H_2 mixture for various gas pressures, we have calculated that the concentration of C_1 species close the substrate is large, and therefore the contribution to the growth rate from these species is no longer negligible, as seen from Fig. 11, especially at lower pressures. Moreover, as the process pressure decreases below 14 Torr the films became NCD/UNCD in nature and this is mirrored by a corresponding increase in our predicted contribution of C_1 species to the growth.

To simulate the data from Ref. 29, the experimental measurements of the filament power consumption were used to find the catalytic dissociation rate Q for different gas pressures p (see Table II). It should be noted that Eq. (6) matches the experimental crystal sizes closely for the range of pressures used (see Fig. 11).

We have also carried out two additional series of calculations with the value of Q halved ($0.5Q$) and doubled ($2Q$) to see the effect of the hydrogen dissociation degree on growth rates. This showed that the growth rates G for all pressures are not significantly affected by these changes in
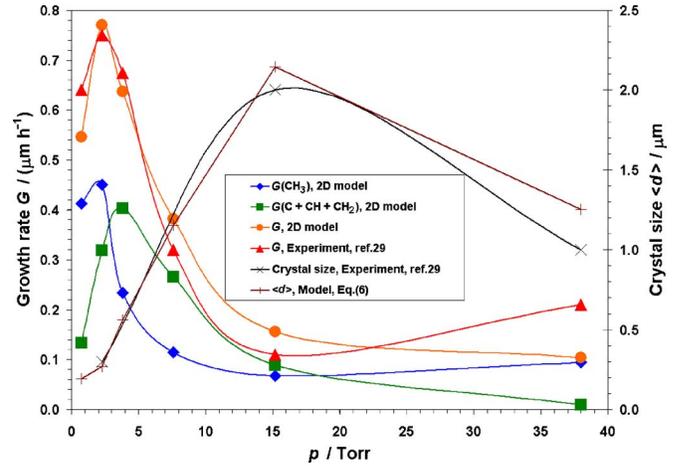
Q. In fact, CH_3 contribution to the growth rate is decreased with increasing Q, while the CH_x ($x<3$) contribution is increased with Q. As a result, total growth rates saturate with H atoms at all pressures under study and the growth rates are almost insensitive to such variations in Q for these particular deposition conditions.

V. CONCLUSIONS

In this article we have presented further evidence to support and refine our model[9,10] for the growth mechanisms of the various forms of diamond film produced in a HF reactor using both $Ar/H_2/CH_4$ and traditional CH_4/H_2 gas mixtures. We have shown that the observed film morphology, growth rate, crystal size, and the variation of these with distance from the filament can be rationalized using a model based on competition to react with dangling bonds on the surface by H atoms, CH_3 radicals, and other C_1 species. A refinement to our previous model is that renucleation depends more critically upon the relative concentrations of H atoms and C_1 species than previously believed.

(i)   If the gas chemistry is such that the concentration of

TABLE II. Values of filament catalytic efficiency, Q, for different pressures, p, calculated for the experimental process conditions of Ref. 29.

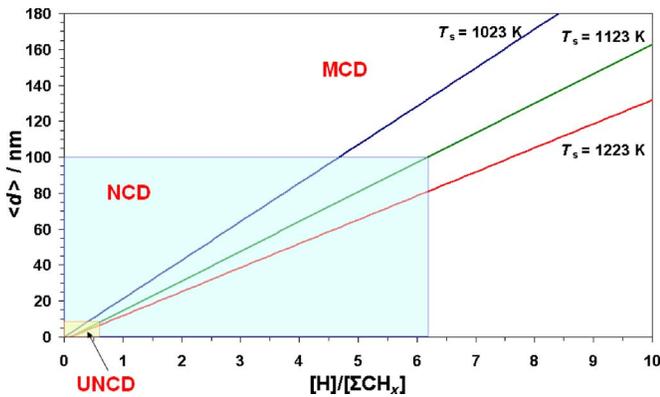| p(Torr)	$Q(10^{19} \text{ cm}^{-2} \text{ s}^{-1})$
0.76	2.9
2.28	4.52
3.8	5.32
7.6	5.76
15.2	6.05
38	5.73

FIG. 12. A plot of average diamond crystal size $\langle d \rangle$ against the ratio of the concentrations of atomic hydrogen to all the other hydrocarbon radicals $\Sigma CH_x(x<4)$ close to the growing diamond surface, for three substrate temperatures, T_s, calculated using Eq. (7). Note that experimentally it is difficult to vary T_s independently of $[H]/[\Sigma CH_x]$, however, this plot serves to illustrate the expected trends. For the purposes of this figure, UNCD has been arbitrarily defined as diamond with crystal size <10 nm, NCD as between $10-100$ nm, and MCD >100 nm, and the various growth regimes are shown as boxes. Extrapolation below $\langle d \rangle = 2$ nm is unreliable since either $[H]$ becomes so small that diamond growth ceases or $[\Sigma CH_x]$ becomes so large that films become graphitic.

C atoms near the surface is high (i.e., comparable with $[CH_3]$), then C atoms can add directly to either a surface radical site (C_d^*) or to a biradical site ($C_d^* - C_d^*$) in direct competition to H addition. This was the case when modeling Schwartz *et al.*'s data,[29] and allowed us to predict their growth rates and crystal sizes very accurately.

(ii)   If the concentration of C atoms near the surface is *not* significantly high (e.g., $[C] \ll 0.1[CH_3]$), nucleation then depends upon the rate of creation of biradical sites, to which CH_3 [as well as CH_x $(x<3)$] radical species can add.

In either case, the mechanism limiting the crystal size could be the growth of the next layer occurring before all the voids of the current layer are filled, which can occur at high CH_3 addition rate,[16] or more exactly, at elevated gaseous $\Sigma CH_x/H$ ratios ($x<4$). For the vast majority of CVD deposition reactors, the ratio of $[H]/[H_2]$ near the substrate is not extremely low, e.g., $[H]/[H_2] > 0.001$ for a typical substrate temperature $T_s = 1123$ K. In this case, the terms in Eq. (6) that are proportional to H_2 concentration can be omitted, giving a simple formula for the average crystal size in nanometers

$$\langle d \rangle = \{2.25 + 0.67 \exp(3430/T_s)\}\{[H]/[\Sigma CH_x]\}. \quad (7)$$

Figure 12 shows the predictions of Eq. (7) for three substrate temperatures, and highlights that the type of film (MCD, NCD, or UNCD) is determined simply by the $[H]/[\Sigma CH_x]$ ratio near the growing diamond surface. Low $[H]/[\Sigma CH_x]$ ratios and elevated substrate temperatures will favor smaller crystal sizes, and thereby promote NCD and UNCD deposition. However, should the atomic H concentration fall too low, then diamond growth ceases ($\langle d \rangle \to 0$), as observed in our and other experiments. Figure 12 is consistent with our previous observations[9] that UNCD deposition occurs in very

narrow range of conditions near the boundary between no-growth and NCD-growth, since this corresponds to a narrow range of $[H]/[\Sigma CH_x]$ ratios. However, it is difficult to test Eq. (7) experimentally since varying T_s affects both $[H]$ and $[\Sigma CH_x]$ near the substrate, and so there is no possibility of independently varying one parameter.

The modeling described in this article has some inaccuracies due to the need to fit the growth rates to a parameter for the filament efficiency, Q. In the MCD regime, the model works quite well and predicts growth rates and crystal sizes reasonably accurately, as evidenced by Fig. 11. However, when the nucleation rate approaches that required for UNCD growth, the model becomes less accurate—although it still predicts grain sizes to within an order of magnitude, as well as the trends in growth rate and grain size with distance from the filament.

Nevertheless, using this model, we have shown that a knowledge of the gas phase concentrations near the growing diamond surface can be used to estimate the growth rate and average crystal size during diamond HFCVD, and thereby to predict whether the film morphology will be MCD, NCD, or UNCD, along with its across-sample uniformity. However, direct experimental measurements of these concentrations close to the growing diamond surface during CVD are urgently required in order to test the accuracy of the model. Also, the modeling needs to be extended to microwave plasma reactors to prove that these proposed growth steps have universal applicability for a variety of growth systems.

ACKNOWLEDGMENTS

[1]P. W. May, Philos. Trans. R. Soc. London, Ser. A **358**, 473 (2000).
[2]S. J. Harris, Appl. Phys. Lett. **56**, 2298 (1990).
[3]D. G. Goodwin and J. E. Butler, in *Handbook of Industrial Diamonds and Diamond Films*, edited by M. A. Prelas, G. Popovici, and L. K. Bigelow (Marcel Dekker, New York, 1998).
[4]*Synthesis, Properties and Applications of Ultrananocrystalline Diamond*, NATO Science Series Part II, Vol. 192, edited by D. M. Gruen, O. A. Shenderova, amd A. Y. Vul' (Springer, New York, 2005).
[5]X. Xiao, J. Birrell, J. E. Gerbi, O. Auciello, and J. A. Carlisle, J. Appl. Phys. **96**, 2232 (2004).
[6]O. A. Williams, M. Daenen, J. D'Haen, K. Haenen, J. Maes, V. V. Moshchalkov, M. Nesládek, and D. M. Gruen, Diamond Relat. Mater. **15**, 654 (2006).
[7]P. W. May, J. A. Smith, and Y. A. Mankelevich, Diamond Relat. Mater. **15**, 345 (2006).
[8]D. Zhou, T. G. McCauley, L. C. Qin, A. R. Krauss, and D. M. Gruen, J. Appl. Phys. **83**, 540 (1998).
[9]P. W. May, J. N. Harvey, J. A. Smith, and Y. A. Mankelevich, J. Appl. Phys. **99**, 104907 (2006).
[10]P. W. May and Y. A. Mankelevich, J. Appl. Phys. **100**, 024301 (2006).
[11]J. R. Rabeau, P. John, J. I. B. Wilson, and Y. Fan, J. Appl. Phys. **96**, 6724 (2004).
[12]Y. F. Zhang, D. Dunn-Rankin, and P. Taborek, J. Appl. Phys. **74**, 6941 (1993).
[13]H. Yamada, A. Chayahara, Y. Mokuno, Y. Horino, and Y. Fujimori, Diamond Relat. Mater. **15**, 522 (2006).
[14]B. W. Yu and S. L. Girshick, J. Appl. Phys. **75**, 3914 (1994).
[15]Y. A. Mankelevich, A. T. Rakhimov, and N. V. Suetin, Diamond Relat.

Mater. **7**, 1133 (1998).

[16]S. Skokov, B. Weiner, and M. Frenklach, J. Phys. Chem. **98**, 7073 (1994).

[17]G. P. Smith *et al.*, http://www.me.berkeley.edu/gri-mech.

[18]Y. A. Mankelevich, N. V. Suetin, M. N. R. Ashfold, J. A. Smith, and E. Cameron, Diamond Relat. Mater. **10**, 364 (2001).

[19]M. N. R. Ashfold, P. W. May, J. R. Petherbridge, K. N. Rosser, J. A. Smith, Y. A. Mankelevich, and N. V. Suetin, Phys. Chem. Chem. Phys. **3**, 3471 (2001).

[20]J. A. Smith, J. B. Wills, H. S. Moores, A. J. Orr-Ewing, Yu. A. Mankelevich, and N. V. Suetin, J. Appl. Phys. **92**, 672 (2002).

[21]A. C. Ferrari and J. Robertson, Phys. Rev. B **63**, 121405 (2001).

[22]G. Leyendecker, J. Doppelbauer, D. Bäuerle, P. Geittner, and H. Lydtin, Appl. Phys. A: Solids Surf. **30**, 237 (1983).

[23]D. S. Dandy and M. E. Coltrin, J. Mater. Res. **10**, 1993 (1995).

[24]*Physical Data*, edited by I. S. Grigoriev and E. Z. Meilihov (Energoat-omizdat, Moscow, 1991), p. 365.

[25]J. B. Wills, M. N. R. Ashfold, A. J. Orr-Ewing, Y. A. Mankelevich, and N. V. Suetin, Diamond Relat. Mater. **12**, 1346 (2003).

[26]Y. A. Mankelevich, N. V. Suetin, M. N. R. Ashfold, W. E. Boxford, A. J. Orr-Ewing, J. A. Smith, and J. B. Wills, Diamond Relat. Mater. **12**, 383 (2003).

[27]S. Skokov, B. Weiner, and M. Frenklach, J. Phys. Chem. **98**, 8 (1994).

[28]Y. K. Liu, Y. Tzeng, C. Liu, P. Tso, and I. N. Lin, Diamond Relat. Mater. **13**, 1859 (2004).

[29]S. Schwarz, S. M. Rosiwal, M. Frank, D. Breidt, and R. F. Singer, Diamond Relat. Mater. **11**, 589 (2002).

[30]L. N. Krasnoperov, I. J. Kalinovski, H. N. Chu, and D. Gutman, J. Phys. Chem. **97**, 11787 (1993).

[31]M. Frenklach (private communication).